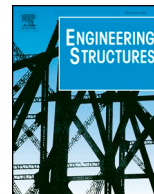




ELSEVIER

Contents lists available at ScienceDirect

Engineering Structures

journal homepage: www.elsevier.com/locate/engstruct

Seismic retrofit of RC buildings using self-centering PC frames with friction-dampers

Mohamed Nour Eldin, Assefa Jonathan Dereje, Jinkoo Kim*

Department of Civil and Architectural Engineering, Sungkyunkwan University, Suwon, Republic of Korea

ARTICLE INFO

Keywords:

Seismic retrofit
Self-centering
Incremental dynamic analysis
Fragility analysis

ABSTRACT

This paper presents the seismic upgrade of existing reinforced concrete (RC) structures by using a self-centering post-tensioned pre-cast concrete frame with friction dampers (SC-PC-FD). The effectiveness of the retrofit is investigated through conducting cyclic loading tests on a single story RC frame before and after the retrofit. The experimental results are used to validate the numerical modeling of the test specimens. A performance-based seismic design procedure is proposed based on a genetic algorithm (GA) to determine the story-wise distribution of the damper friction capacity and the area of post-tensioning steel. Three-, five-, and eight-story RC framed structures are used as case study models for evaluating the effectiveness of the retrofit technique. Non-linear time-history response analysis (NLTHA), incremental dynamic analysis (IDA), and fragility analysis are conducted to investigate the seismic performance of the retrofitted structures. Results of the nonlinear time-history analyses show that the retrofit reduces the maximum inter-story drift ratio (MIDR) and the residual drift of the model structures. IDA and fragility curves show that the collapse capacities of the model structures are increased after the retrofit and the retrofitted buildings have lower probabilities of reaching the design limit states compared to the un-retrofitted ones.

1. Introduction

After strong earthquakes, building authorities and owners search for the fastest and most reliable methods for recovering the functionality of buildings. Recently, the research community realized that designing a building to survive a design-based earthquake is necessary but may not be sufficient to recover the initial condition and functionality of structures, especially, if the structure is subjected to significant structural damage or excessive residual drift. To reduce earthquake-induced residual drift, the concept of self-centering systems has emerged as a new trend for seismic retrofit of structures [1–3]. Using a self-centering system keeps a structure responding elastically under design-level earthquake and reduces or eliminates the residual drift. Post-tensioned elements are generally used to achieve the self-centering ability.

Sometimes easily replaceable energy dissipation components are added to absorb seismic energy. The combination of the self-centering and energy dissipative devices provides a flag-shaped hysteresis behavior that enhances the efficiency of the lateral resisting system of the structure during ground excitations.

The concept of self-centering has been applied to steel structures [4,5], RC structures [6], and timber structures [7,8]. Many studies investigated the performance of self-centering systems; for example, Song et al. [9] proposed a self-centering prestressed concrete (SCPC) moment-resisting frame (MRF) with web friction devices (WFDs). In their proposal, aluminum plates are used for friction and post-tensioned tendons are replaced by a bundle of tendons to facilitate the field assembly. Eatherton et al. [5] tested a half-scale rocking braced steel frames that use column-uplifting mechanisms, high-strength post-tensioned

Abbreviations: RC, reinforced concrete; SC-PC-FD, self-centering post-tensioned pre-cast concrete frame with friction dampers; GA, genetic algorithm; NLTHA, non-linear time-history response analysis; IDA, incremental dynamic analysis; MIDR, maximum inter-story drift ratio; PC, pre-cast concrete; PT, post-tensioned; FD, friction damper; LVDT, linear variable differential transformer; PC-FD, precast-cast frame with friction damper; DBE, design-basis earthquakes; IO, immediate occupancy; LS, life-safety; CP, collapse prevention limit state; MCE, maximum-considered earthquake

* Corresponding author.

E-mail address: jkim12@skku.edu (J. Kim).

<https://doi.org/10.1016/j.engstruct.2019.109925>

Received 21 August 2019; Received in revised form 8 November 2019; Accepted 11 November 2019

Available online 21 November 2019

0141-0296/ © 2019 Elsevier Ltd. All rights reserved.

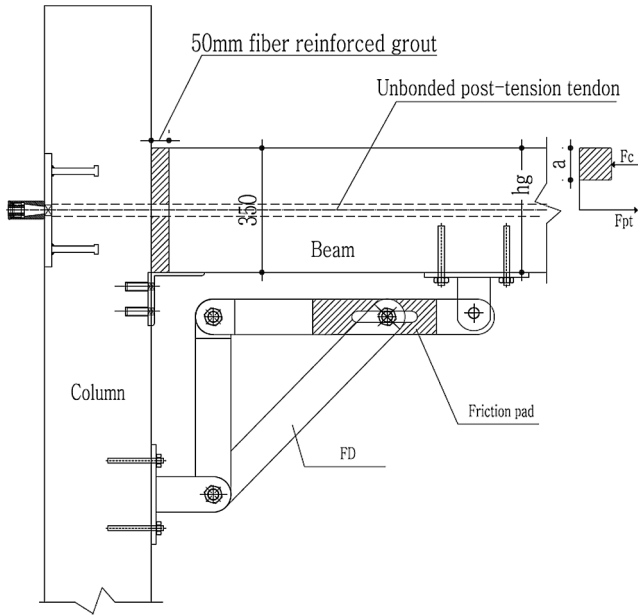


Fig. 1. Beam-column interface of the SC-PC retrofit frame.

oning, and replaceable energy-dissipating fuses. Through conducting quasi-static cyclic tests, they demonstrated that the controlled rocking system could satisfy the required performance goals. Cao et al. [10] proposed an iterative procedure to describe the deformation of dissipators of a self-centering prestressed concrete (SCPC) bridge pier with external dissipators under different conditions. Guo et al. [11] upgraded existing frame structures by using the self-centering (SC) concrete wall with friction dampers. Dezfuli et al. [12] conducted a parametric study on an innovative Core-Less Self-Centering (CLSC) brace (i.e. a retrofit device to be used in conjunction with conventional lateral resisting systems). Wang and NourEldin et al. [13] proposed a retrofit design procedure for existing structures using self-centering post-tensioned pre-cast concrete (SC-PC) frames utilizing the initial stiffness and enlarged beam ends. Morelli et al. [14,15] conducted experimental and numerical studies on the capacity of reducing the residual deformation of existing steel structures by using re-centering devices with post-tensioned and replaceable energy-dissipating elements.

In this paper, a pre-cast concrete PC frame with self-centering and energy dissipating capability is developed for seismic retrofit of existing

RC buildings. Cyclic loading tests are conducted on a single story RC frame before and after the retrofit to examine the effectiveness of the proposed retrofit system. The experimental results are used to validate the numerical modeling of the test specimens. A performance-based seismic design based on a genetic algorithm is proposed for the effective application of the retrofit system. Three-, five-, and eight-story RC frames are used as case study buildings, and the seismic performance of the structures is assessed through incremental dynamic analysis and fragility analysis.

2. Analytical modeling of the seismic retrofit system

The retrofit system is composed of PC columns and beams connected by post-tensioned tendons (Fig. 1) and rotational friction dampers installed at the corner. The stress-strain relation of the post-tensioning tendon recommended by Mattock [16] for Grade 270 prestressing strands is given by

$$f_{pt} = \varepsilon_{pt} \cdot E_p \cdot \left[0.02 + 0.98 \left/ \left[1 + \left(\frac{\varepsilon_{pt} \cdot E_p}{1.04 \cdot f_{py}} \right)^{8.36} \right]^{1/8.36} \right. \right] \quad (1)$$

where f_{pt} and ε_{pt} are the stress and strain in the post-tensioning tendon, E_p is the elastic modulus of the tendon, and f_{py} is the yield strength of the post-tensioning tendon.

The moment capacity of the beam-column connection, M_{cap} , is calculated by multiplying the force developed in the post-tensioning tendon, F_{pt} , with the distance to the resultant concrete compression force, F_c , as shown in Fig. 2. From equilibrium,

$$F_c = F_{pt} \quad (2)$$

Based on that, the moment capacity of the beam-column connection is obtained as follows:

$$M_{cap} = F_{pt} \cdot (h_g - a) / 2 \quad (3)$$

where h_g is the height of the grout pad at the beam-column interface; a is the depth of the equivalent rectangular compression stress block corresponding to the compression force, which can be determined using the following equation [17]:

$$a = F_c / 0.85 f'_c b_g \quad (4)$$

where F_c is the concrete compression force; b_g is the width of the grout pad at the beam-column interface; f'_c is the unconfined concrete compression strength.

At the yield of the post-tensioning tendon, M_{cap} can be calculated as

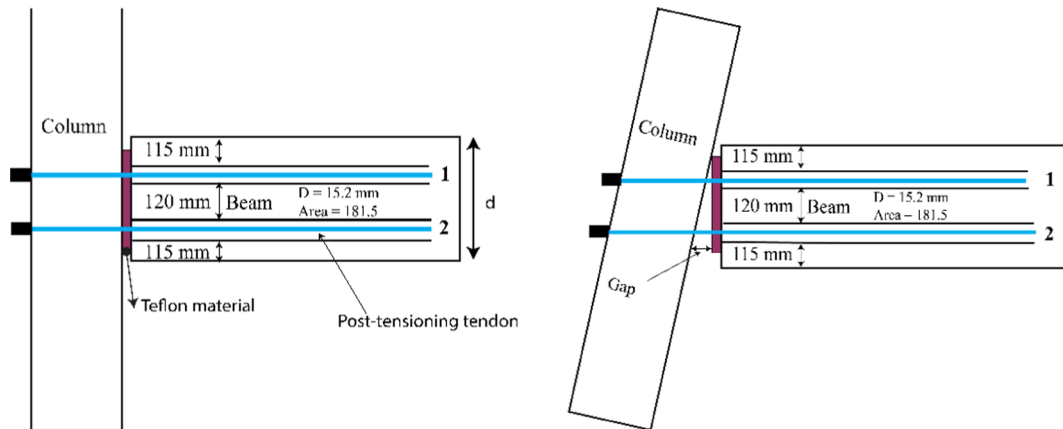


Fig. 2. Beam-column interface of the PC frame used in the test and analysis before and after gap opening.

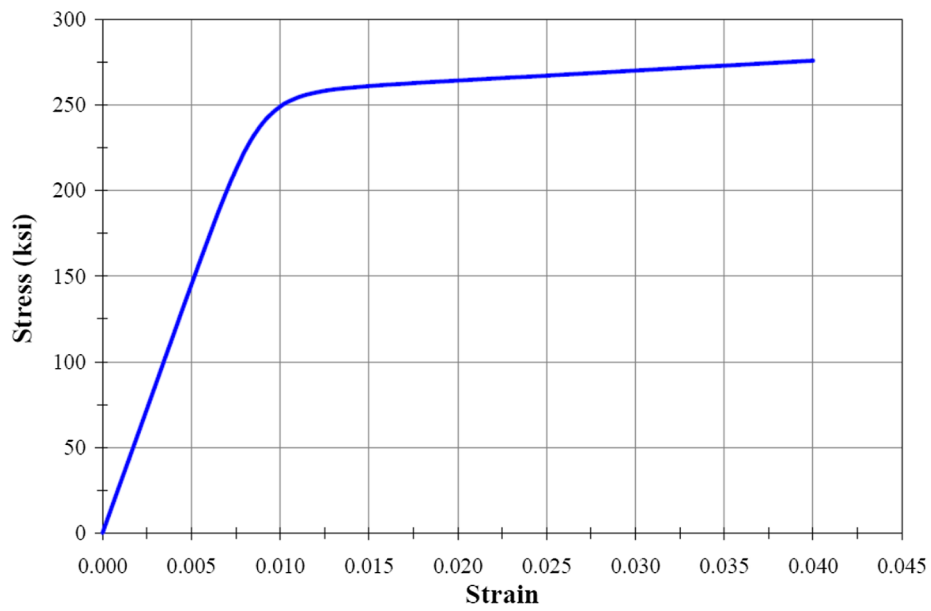


Fig. 3. Stress-strain curve of Grade 270 prestressing strands.



(a) Friction damper (FD) installed at the corner of the PC frame.



(b) Experiment setup for the FD

Fig. 4. Rotational friction damper developed for the current study.

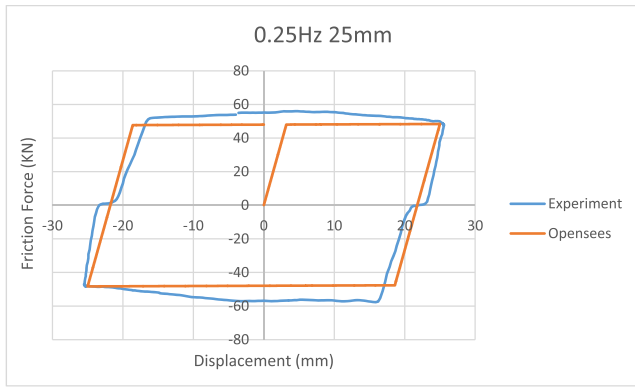
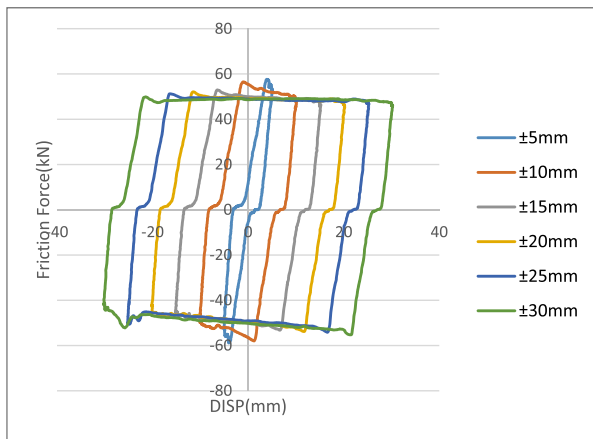
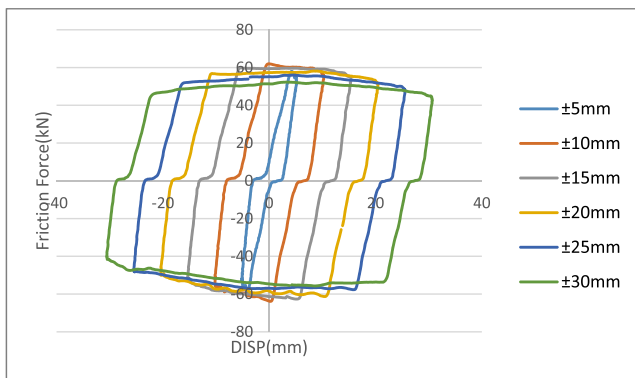


Fig. 5. Hysteresis loops of the FD obtained from the experiment and the analytical modeling.



(a) Frequency=0.125 Hz



(b) Frequency=0.25 Hz

Fig. 6. Hysteresis curves of the FD under different amplitudes and loading frequencies.

$$M_{cap} = F_{py} \cdot (h_g - a) / 2 \tag{5}$$

The decompression point defines the beginning of a gap opening at the connection interface and corresponds to the condition when the stress in the extreme concrete compression fiber reaches zero at the beam-end adjacent to the column. Accounting for the precompression introduced by the initial prestressing force, and assuming a linear strain distribution at the critical section, the following equation is used to determine the moment resistance at gap opening, M_{decomp} [18].

$$M_{decomp} = f_{pi} \cdot I / \left(\frac{h_g}{2} \right) \tag{6}$$

where f_{pi} is the initial stress in the post-tensioning tendon, I is the moment of inertia of the beam section based on the gross section properties, and h_g is the height of the grout pad at the interface.

At the beam-column interface, a bi-linear elastic spring is used where the gap opening starts between the column and the beam at the decompression level in the post-tensioned (PT) tendons. When the applied moment exceeds M_{decomp} , the gap opens and the PT tendons start to elongate. In this study, two tendons are placed in each beam of the PC frame test specimen to produce restoring force. Fig. 2 shows the beam-column interface of the PC frame used in this study before and after gap opening and Fig. 3 shows the stress-strain curve of the Grade 270 strand.

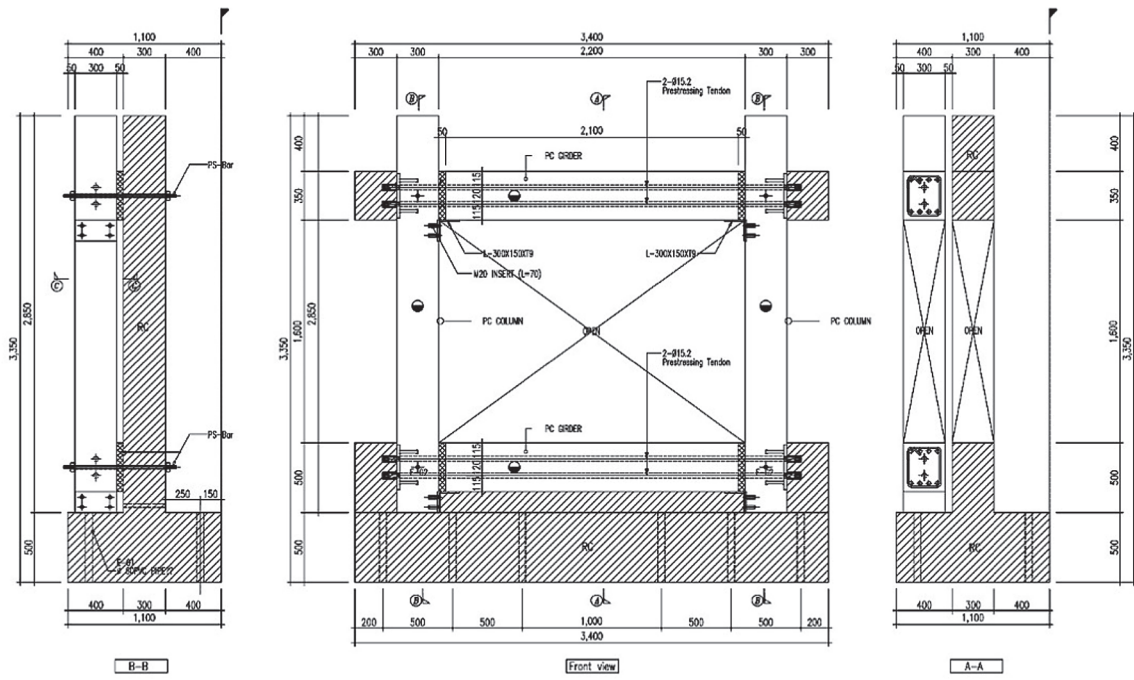
3. Analysis modeling of corner friction dampers

A friction damper (FD) is developed to be placed at the corner of the PC frame as shown in Fig. 4(a). In order to test the clamping force required to generate the intended damper yield capacity, a friction damper is tested under cyclic load as shown in Fig. 4(b). A friction pad is used to generate the friction force between the steel elements at the slotted and knee parts. Torques of 600 and 450 Nm are used at the slotted and knee parts, respectively, with a corresponding clamping force of 135 and 100 kN.

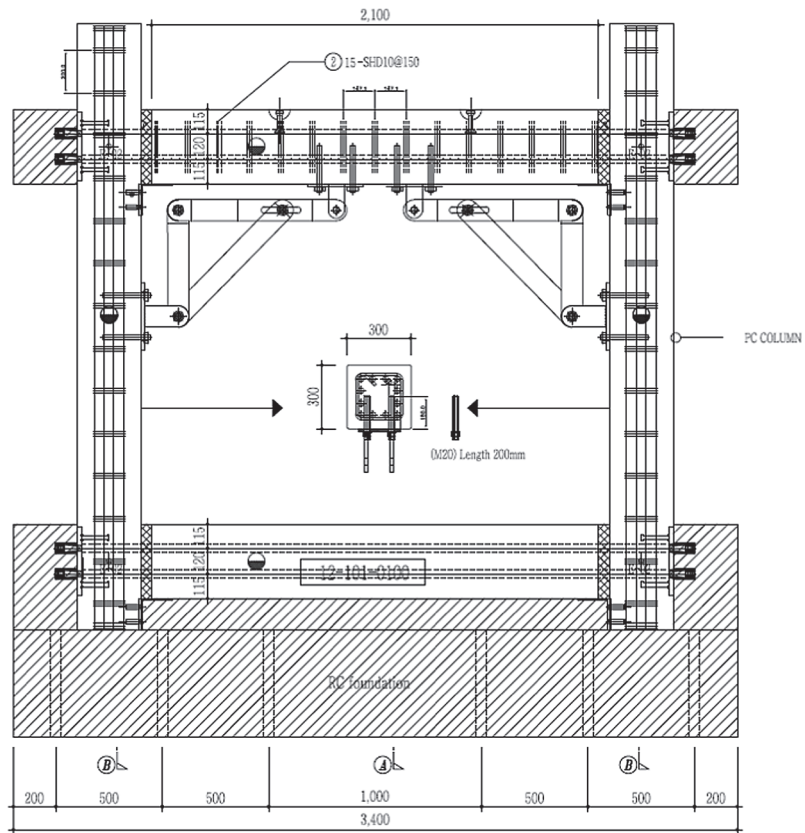
The force-deformation relationship of the friction damper (FD) is tested experimentally and is fitted with an analytical model using the Open System for Earthquake Engineering Simulation (OpenSees) [19] as shown in Fig. 5. The friction damper is modeled with an element having an elastic perfectly plastic hysteretic behavior selected from the OpenSees library. In order to check the yield capacity and the hysteretic performance of the FD, multiple cyclic loading tests have been conducted using different loading frequency, velocity, and displacement amplitudes. Fig. 6 shows the hysteresis curves of the FD under the loading frequency of 0.125 and 0.25 Hz. As can be seen, the FD shows stable hysteresis curves up to 30.0 mm displacement for both load frequencies. In addition, the FD yield force is found to have a lower bound around 50.0 kN for the given loading frequencies. It is observed that the FD yield force is slightly higher for higher frequency (0.25 Hz) loading compared to that for lower frequency loading (0.125 Hz). The reason for this difference may be attributed to the effects of the wear and the heat, which increase when the time for completing one cycle become larger.

4. Configuration of the test specimens

Fig. 7 shows the dimension and configuration of the RC bare frame

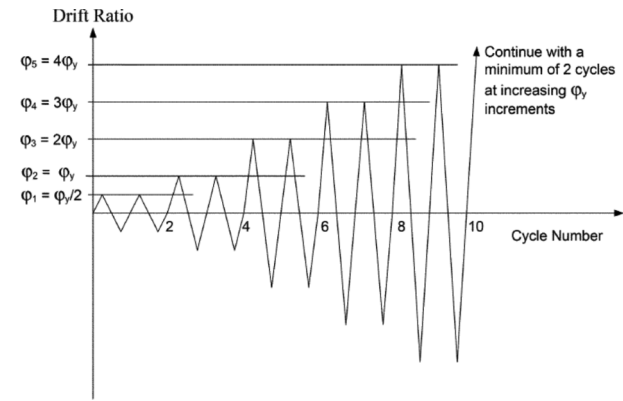


(a) PC frame attached to the RC frame

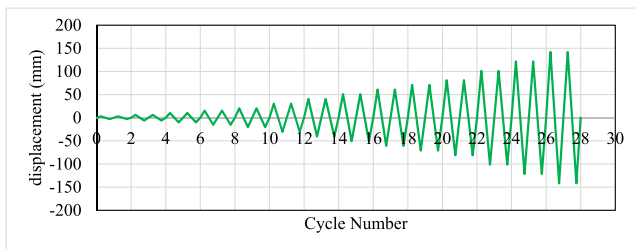


(b) PC frame with FD

Fig. 7. Dimensions and configuration of the test specimens.



(a) Loading protocol recommended in ACI 374.2r-13



(b) Loading protocol used in the experiment.

Fig. 8. Loading protocol for cyclic loading test.

test specimen and the PC frame to be used for seismic retrofit. The cross-sections of the columns and beams of the RC frame are 300×300 mm and 300×350 mm, respectively. Eight rebars having 22 mm diameter are used as main reinforcement for both columns and beams. Shear reinforcement is made with 10 mm stirrups every 200 mm and 150 mm for columns and beams, respectively. The columns and beams of the PC frame have a size of $300 \times 300 \times 2850$ mm and $300 \times 350 \times 2100$ mm, respectively. Two PC beams are placed at the top and bottom of the PC columns as shown in the figure. The reinforcement of the PC column consists of twelve of 22 mm rebars with 10 mm diameter stirrups spaced at every 200 mm. The beam reinforcement of the PC frame consists of six 22 mm rebars (three each at top and bottom) with 10 mm stirrups at a 150 mm interval. A 50.0 mm Teflon plate is inserted at the interface between the PC beams and columns. Steel seat angles are used for positioning the PC beam during the erection and pre-tensioning of the tendon.

The pre-stressing seven-wired tendon (diameter of 15.2 mm) has a yield strength of 1600 MPa and 146 kN pre-tensioning force. The concrete compressive strength for RC and PC frames is 22 and 40 MPa, respectively. The reinforcement steel yield strength for RC and PC frames are 400 and 500 MPa, respectively. The PC frame is connected to the RC frame using horizontal anchor rods (with 32.0 mm diameter and yield strength of 930 MPa) that penetrate the beam-column joints of the two frames. A 50.0 mm Teflon plate is inserted at the interface of the two frames to prevent friction. The PC-frame columns are not connected to the base and there is a sufficient tolerance maintained between the bottom of the PC-columns and the top of the base during the test. This is required to avoid any resistance to the column rotation during the test.



(a) Bare RC frame



(b) Retrofitted frame



(c) Friction dampers

Fig. 9. Test setup for cyclic loading tests.

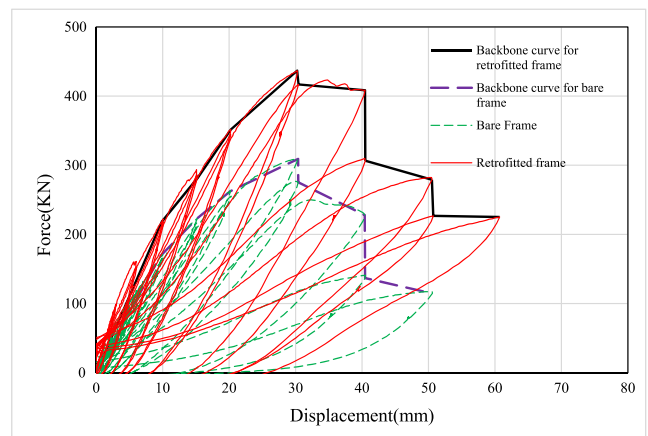


Fig. 10. Hysteresis curves of the RC frame before and after retrofit.

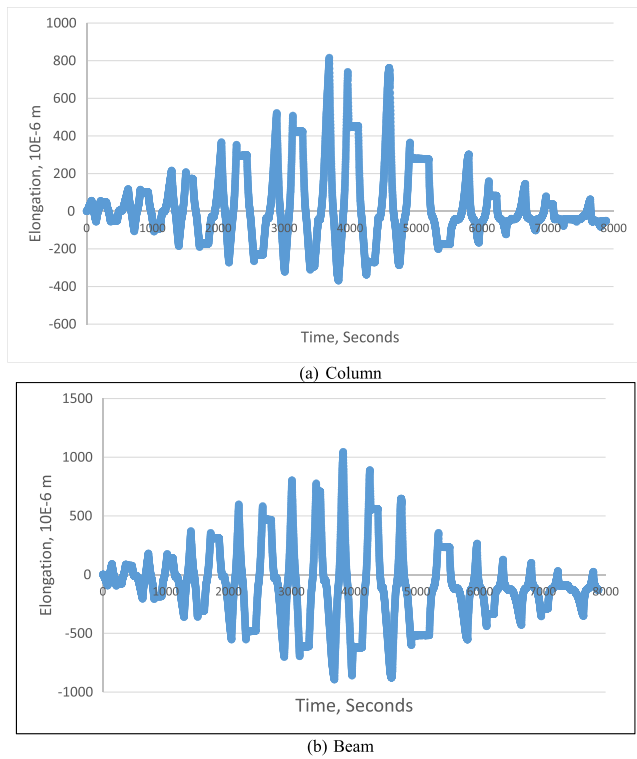


Fig. 11. Strain time histories of the longitudinal reinforcement bars in the column and the beam.

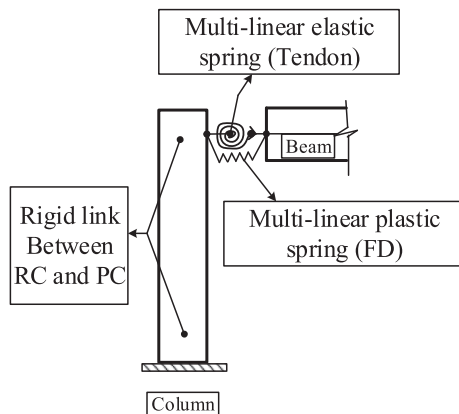
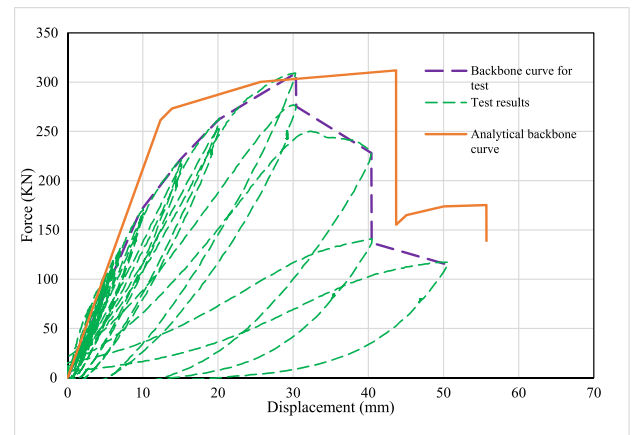


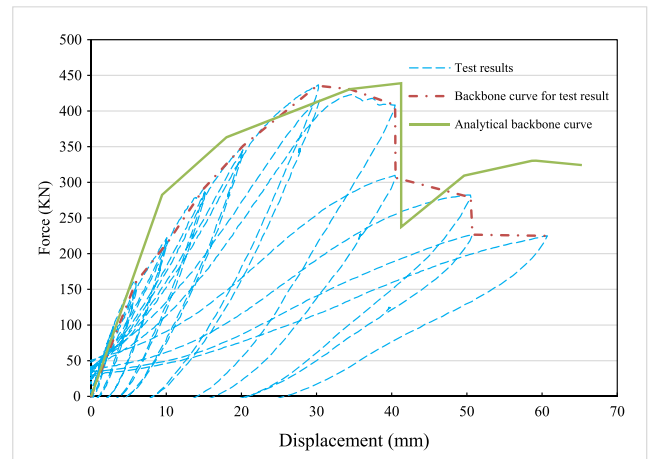
Fig. 12. Analysis model of the PC-FD frame.

5. Cyclic loading test of the specimens

Displacement-controlled cyclic tests of the specimens before and after the seismic retrofit are carried out using a 2000 kN hydraulic servo actuator to evaluate their seismic performance. Strain gauges are attached to the steel rebars of the RC frame at different locations. LVDTs (linear variable differential transformer) are installed to measure the horizontal displacement at the upper part of the specimens during the



(a) Backbone curve before retrofit



(b) Backbone curve after retrofit

Fig. 13. Backbone curves of the RC frame before and after the retrofit.

loading test. The loading protocol used in the test, shown in Fig. 8(b), is constructed based on the loading protocol for the quasi-static cyclic tests recommended in the ACI 374.2r-13 [17] shown in Fig. 8(a). Fig. 9 shows the test setup for the retrofitted RC frame and bare RC frame specimens. The hydraulic actuator is fixed to a rigid concrete wall and is connected to a data acquisition system to plot a real-time force-displacement relation of the actuator.

Fig. 10 shows the hysteresis curves of the RC frame before and after retrofit obtained from the experiments. The figure shows that the retrofitted frame has larger stiffness compared to the bare frame, and has about 40% larger strength in comparison with the bare frame. It is observed that the first drop in strength for both frames occurs at 30.0 mm (i.e. 1.5% of the inter-story drift of the frame height). In addition, the ultimate collapse is reached at 50.0 mm lateral displacement in the case of the bare frame, and at 60.0 mm for the retrofitted frame (i.e. 20.0% increase in displacement at total collapse). The displacements at zero force level in the hysteresis curves represent the amount of energy dissipation due to inelastic deformation, which is larger in the retrofitted case because of the friction dampers and the tendons. The strain time histories recorded by the strain gauges attached to the longitudinal reinforcement bars in the column and the beam of the RC frame are shown in Fig. 11.

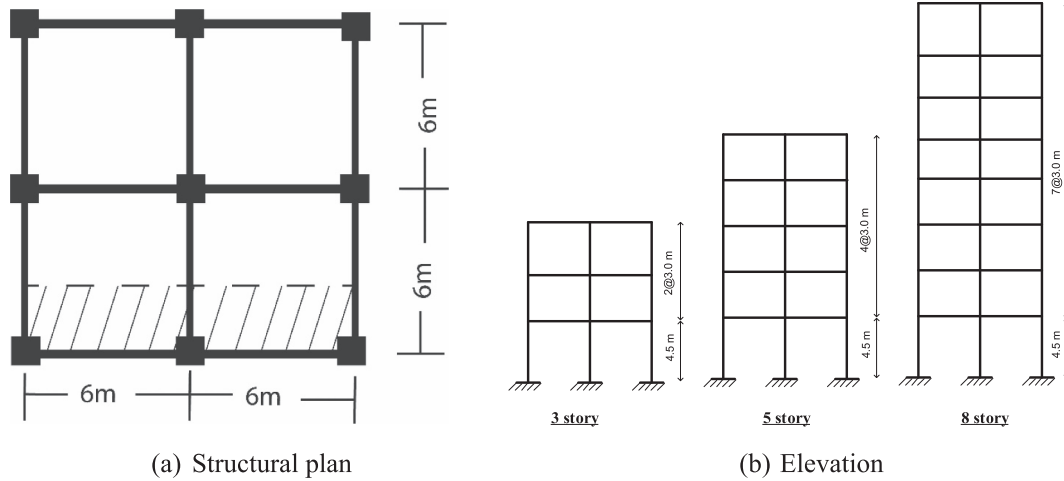


Fig. 14. Configuration of the RC analysis model frames.

Table 1
Reinforcement details of the RC analysis model structures.

Model	Dimensions (mm)	Longitudinal Reinforcement		
		Top	Bottom	Transverse
(a) Beams				
3, 5, and 8-story	250 × 400	4 D20	4 D20	D8, 2legs@150 mm
(b) Columns				
Model	Dimensions(mm)	Longitudinal Reinforcement		Transverse
3-story	300 × 300	6 D14		D8, 2legs@150 mm
5-story	400 × 400	8 D16		
8-story	450 × 450	12 D16		

Fig. 12 shows the analytical modeling of the PC-FD frame, and Fig. 13 depicts the comparison between the numerical and experimental backbone curves of the RC frame before and after the retrofit. The numerical backbone curves of the specimens are obtained using SAP2000 [20] software. A multi-linear elastic spring is selected from the SAP2000 library to model the post-tensioned tendons. A multi-linear plastic spring is used to model the FD that is located at the beam-column connection of the PC frame. The columns of the RC frame are fixed at the bottom and a rigid link is used to model the anchor bolt that connects the RC and PC frames. Frame elements in SAP2000 are used to model the RC beams and columns considering the longitudinal and shear reinforcement. Plastic hinges are assigned at the ends of the RC beams and columns to account for the non-linear behavior. The parameters of the plastic hinges are determined based on the recommendations of ASCE/SEI-41 [22]. The figure shows that, for both the retrofitted and bare frames, the initial stiffness obtained numerically is almost the same as that obtained experimentally. The backbone curve of the experiments shows a smooth transition between the linear and non-linear range before the drop of strength. On the other hand, the

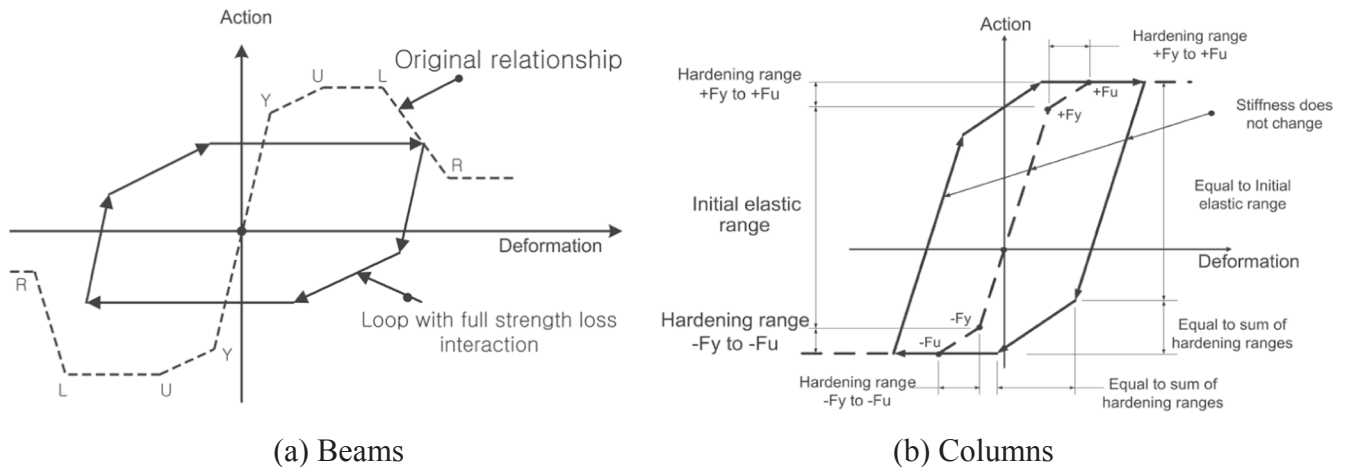


Fig. 15. Hysteresis loops of the RC beams and columns used in the non-linear analysis.

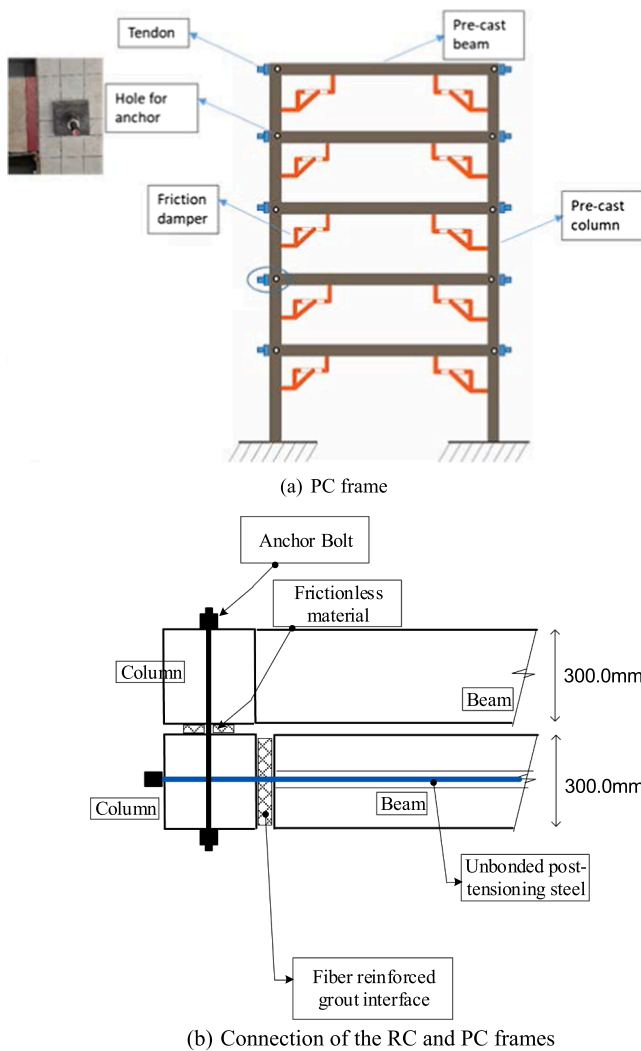


Fig. 16. Components of the PC frame and its attachment to the RC frame.

analytical backbone curve shows a sharp transition between the linear and the non-linear range. This is attributed to the limitation of the numerical iteration algorithm related to the non-linear static analysis in the SAP2000 software, in which the tangent stiffness cannot be represented accurately in this transition zone. In the bare frame specimen, the experimental strength drops from 305 kN to 275 kN at 30.0 mm lateral displacement. The strength of the analytical backbone curve, however, drops from 305 kN to 150 kN at 44.0 mm lateral displacement. In the case of the retrofitted frame, the strength drops from 440 kN to 300 and 238 kN for the experimental and the analytical backbone curves, respectively. After the strength drop, the analytical and experimental results do not match well due to the numerical instability and convergence problems of the analysis algorithm.

6. Seismic retrofit of example buildings

In this section, the effectiveness of the PC retrofit frame is investigated using different RC framed structures. The seismic retrofit for

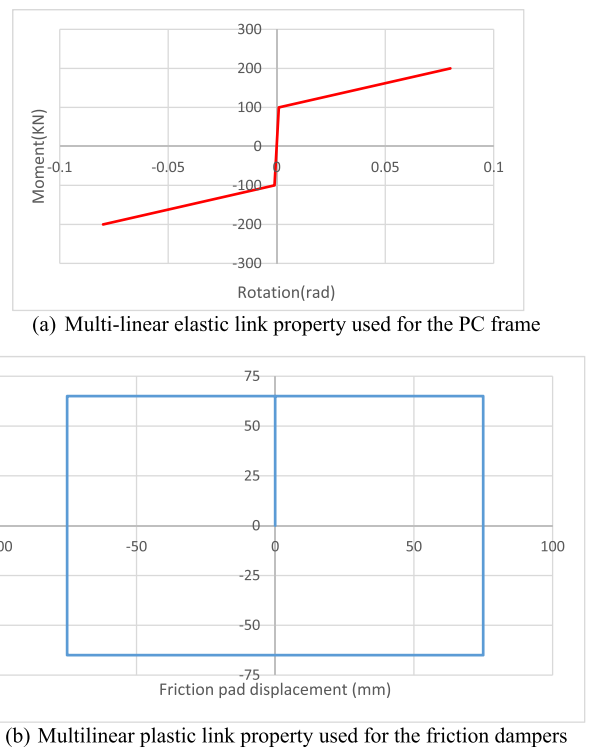


Fig. 17. The analytical model of the retrofit system.

these buildings is achieved by adding the preloaded PC frames externally at the outer perimeter of the frames in the required direction.

6.1. Design and analytical modeling of the RC buildings and the PC frames

Fig. 14 shows the plan and elevations of the analysis models. One of the exterior RC moment frames of the building is separated for simplicity in nonlinear analysis. The building is designed for a dead load of 4.1 kN/m² and a live load of 2.5 kN/m². ACI 318 [21] is used for the design of the RC elements. The dimensions and reinforcement of the RC elements are presented in Table 1. The compressive strength of the concrete is taken as 20.7 MPa (3000 psi) and grade 60 (413 MPa yield strength) steel used for the reinforcement bars. The moment of inertia of the beam and the column sections are reduced to 35% and 70% of those of nominal un-cracked values, respectively, to account for the cracked condition of the elements according to ACI 318. For modal and dynamic analyses, 5% of the critical damping is used. Plastic hinges defined based on ASCE/SEI 41-13 [22] are introduced at the ends of the beams and columns to account for the material non-linearity. According to the modal analysis, the fundamental periods of the 3, 5, and 8-story RC frames are found to be 0.87 s, 1.2 s, and 1.9 s, respectively. The hysteresis loops of the beams and columns used in the dynamic analysis are shown in Fig. 15. A rigid connection is assumed between beams and columns, and the first story columns are assumed to be fixed to the ground.

Fig. 16 shows the components of the PC frame, where the beams are modeled as member elements with a multi-linear elastic link at both ends as shown in Fig. 12(a). The multi-linear elastic link property used for the PC frame is depicted in Fig. 17(a). The columns are modeled as

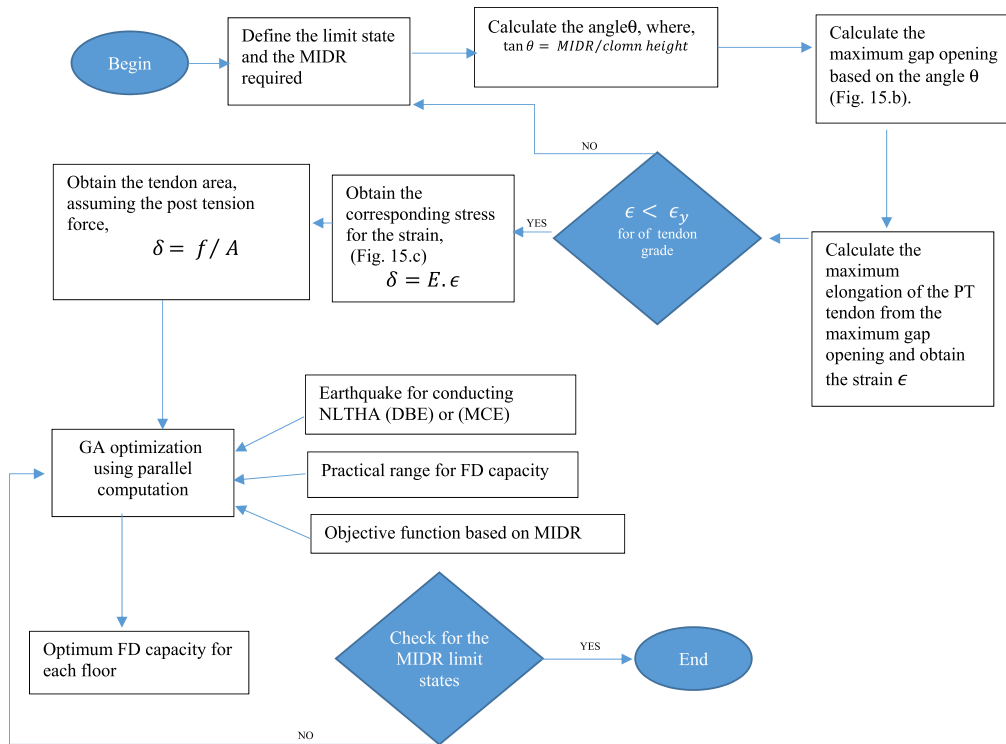


Fig. 18. Design procedure for the PC retrofit.

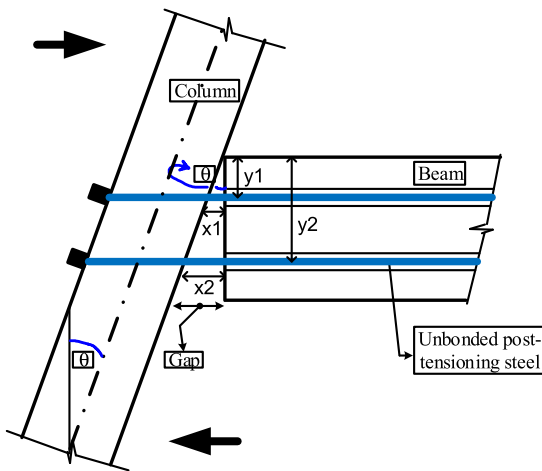


Fig. 19. The geometry of the deformed PC frame.

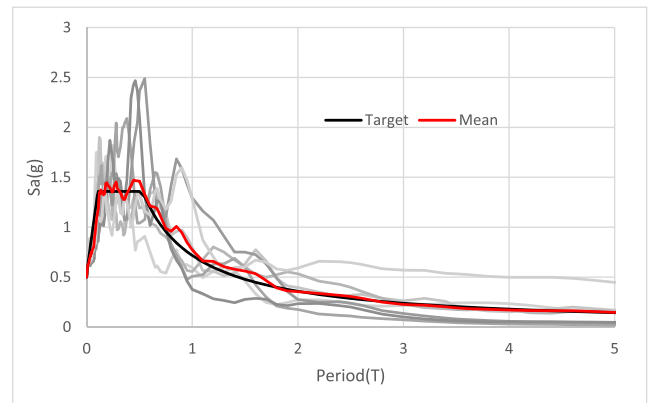


Fig. 21. Target spectrum and response spectra of the seven earthquakes scaled to the target spectrum.

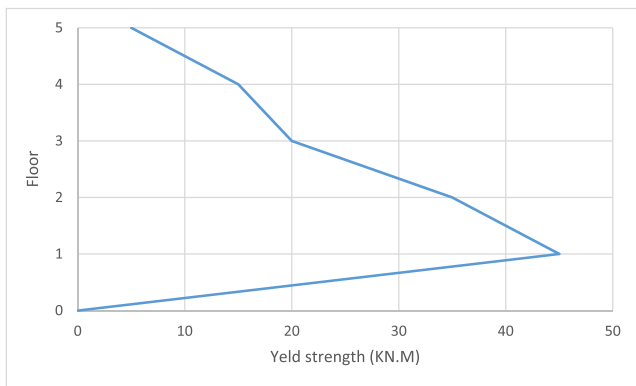


Fig. 20. Vertical distribution of yield force of friction dampers obtained from genetic algorithm.

member elements and are fixed at the base. The friction damper is modeled using a multilinear plastic link which has the property shown in Fig. 17.

6.2. Proposed seismic retrofit procedure

In the current study, a performance-based seismic design procedure is applied for selected earthquakes (design-basis earthquakes (DBE) or maximum considered earthquakes (MCE)). For the design of friction dampers, a genetic algorithm (GA) is applied to determine the optimum yield force of the friction damper installed in each story. As GA is a probability search methodology, the optimum values are generally derived after a certain number of generations. If the solution is not as expected or the objective function does not meet certain criteria, the

Table 2
List of the earthquake records used in the nonlinear dynamic analysis.

Sequence Number (PEER)	Earthquake Name	Station Name	Magnitude	PGA (g)	Source distance (km)	Fault type	Tp (pulse period-sec)
68	“San Fernando”	“LA - Hollywood Stor FF”	6.61	0.231	22.77	Reverse	–
169	“Imperial Valley-06”	“Delta”	6.53	0.240	15.82	strike slip	–
721	“Superstition Hills-02”	“El Centro Imp. Co. Cent”	6.54	0.358	22.03	strike slip	–
752	“Loma Prieta”	“Capitola”	6.93	0.515	12.56	Reverse Oblique	–
953	“Northridge-01”	“Beverly Hills – 14,145 Mulhol”	6.69	0.448	18.2	Reverse	–
1111	“Kobe_ Japan”	“Nishi-Akashi”	6.9	0.490	11.16	strike slip	–
1244	“Chi-Chi_ Taiwan”	“CHY101”	7.62	0.340	15.23	Reverse Oblique	5.341

number of generations may be modified or the initial input values are changed.

The proposed retrofit procedure upgrades the existing building by attaching the preloaded PC frame to the outer perimeter of the building. The design objective of the retrofitted building is set up to satisfy a specific limit states (e.g. immediate occupancy (IO), life-safety (LS), or collapse prevention (CP) limit state). At a certain level of the limit state, gap opening or decompression in tendons takes place at the joint between the PC beams and columns, and the maximum inter-story drift ratio (MIDR) should be maintained below the required limit values. Fig. 18 shows the flowchart of the proposed procedure, which can be summarized in the following steps:

1. The maximum inter-story drift ratio (MIDR) is defined based on the limit state required. For example, MIDR = 2.0% for the collapse prevention limit state.
2. From the geometry of the PC frame, the rotational angle (θ) corresponding to the MIDR is calculated at the bottom of the PC column by

$$\tan\theta = \text{MIDR}/\text{column height} \quad (7)$$

3. The maximum elongation in each PT tendon of the PC beams is calculated using θ , PC beam depth, and the depth of the PT from the top of the PC beam as follows (Fig. 19)

$$x_1 = y_1 \cdot \tan\theta \quad (8)$$

$$x_2 = y_2 \cdot \tan\theta \quad (9)$$

4. The strain and stress induced in the PT tendon are computed as follows

$$\epsilon = (x_1 + x_2)/L \quad (10)$$

$$\delta = E \cdot \epsilon = F/A \quad (11)$$

where ϵ is the tendon strain which should be less than the yield strain of the tendon ($\epsilon < \epsilon_y$), δ is the tendon stress, E is tendon Young's modulus, F is the post-tensioning force, and A is the tendon cross-sectional area. The post-tensioning force can be assumed and the corresponding cross-sectional area of the tendon can be obtained.

5. A genetic algorithm optimizer is used to obtain the optimum capacity of the friction dampers at each floor of the building. An earthquake record scaled to DBE or maximum-considered earthquake MCE is used for conducting non-linear time history analysis (NLTHA) for GA in each generation. In this study parallel computing is used to reduce computational time. Any simplification for analysis

modeling of the retrofitted building is permitted as long as it preserves the dynamic characteristics of the structure. The MIDR can be used as an objective function or a constraint, and the initial cost can be set as another objective function.

6. The final check is made by conducting dynamic analysis on the retrofitted building using the earthquake records scaled to DBE or MCE spectrum and confirming that the final MIDR is within the allowed limits. If not, the yield capacity of the friction damper is increased in the same proportion until the required MIDR is satisfied.

For the present study, the yield strength of the post-tensioning tendons, f_{py} , is set to be 1600 MPa and the initial stress after losses, f_{pi} , is 820 MPa; the nominal compressive concrete strength, f'_c , is 20.7 MPa. Two tendons are used for each PC beam as in the case of the experiment. The retrofit frame is connected with the bare frame at each floor to maintain a rigid diaphragm at each level. Guidelines for such a type of connection is given elsewhere [23].

The practical range of the friction damper (FD) capacities selected in this study to obtain the optimum value in the GA optimization is between 5 and 50 kN, varied with 5 kN interval. It has been found that for the building under investigation, the vertical distribution of the FD yield force follows a triangular pattern starting from the largest value at the first story and decreasing toward the upper floors. This finding is true regardless of the number of generations used during the GA process. For example, for the 5-story building, the distribution of the FD yield force is investigated for 20 and 76 generations. The 20 generations involve 400 nonlinear dynamic analyses and 76 generations involve 1520 analyses using parallel computing. The optimum FD yield force is found to be 45, 35, 20, 10, and 5 kN, respectively, for the 1st, 2nd, 3rd, 4th, and 5th stories as shown in Fig. 20. This is true for both generations, except for the 4th story where the optimum value is found to be 15kN for the 76 generations. A similar finding has been highlighted in previous studies [24].

6.3. Seismic performance evaluation of the retrofitted structure

In this section, the seismic performance of the retrofitted structures is evaluated using nonlinear dynamic analyses. The site class soil-profile for earthquake records used in the analysis is assumed to be SD (weak soil), and the spectral accelerations at short periods and at one second are $S_{DS} = 0.70$ g and $S_{D1} = 0.38$ g, respectively, based on ASCE 7-16 [25] format. The earthquake level is assumed to be the maximum considered earthquake (MCE) level for the given site. Seven earthquake records compatible with the design response spectrum, Fig. 21, are used for conducting the dynamic time-history analyses. Table 2 gives the details of the seven earthquake records. The seismic performance of the

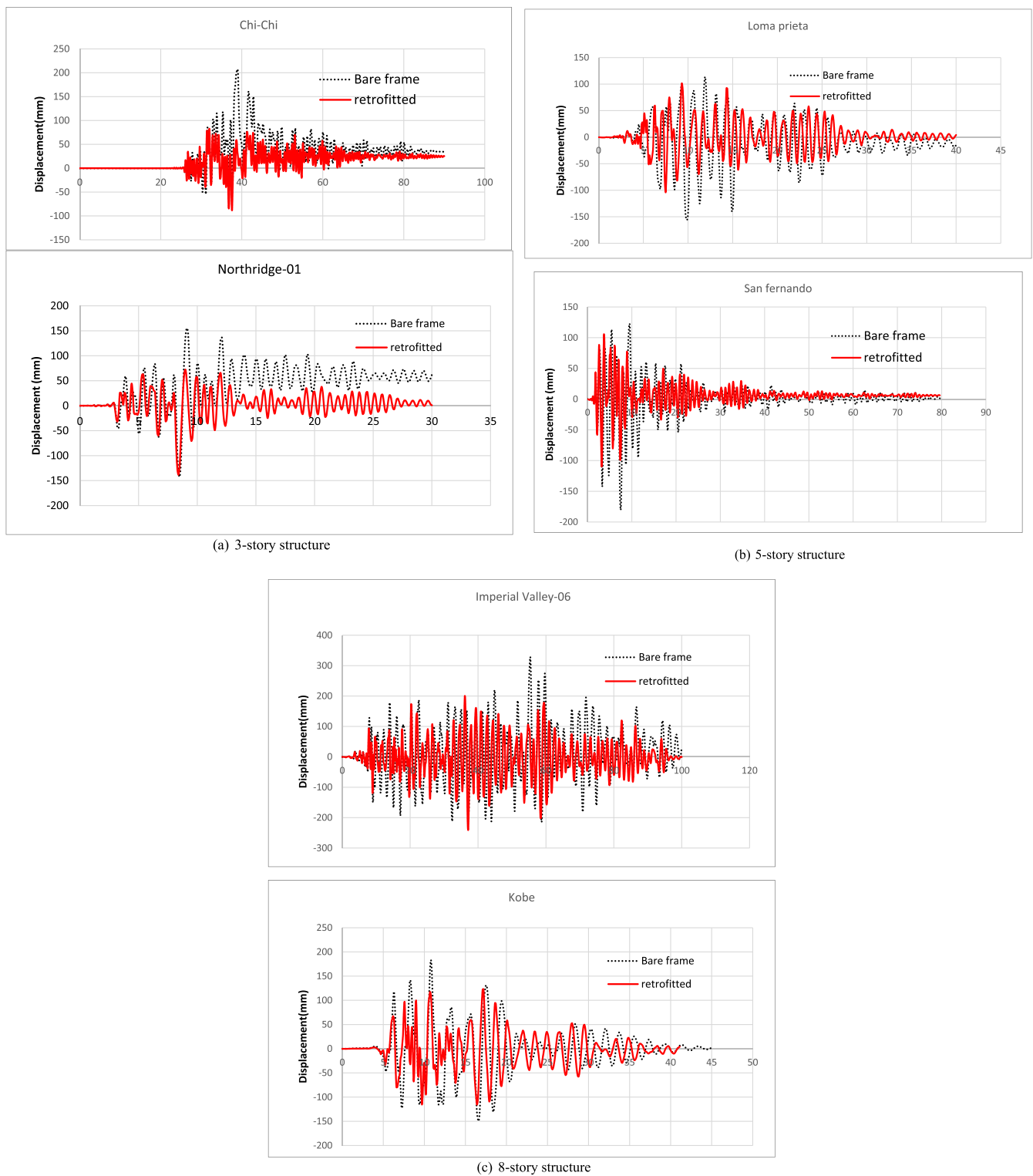


Fig. 22. Roof story displacement time history of the example structures before and after the seismic retrofit.

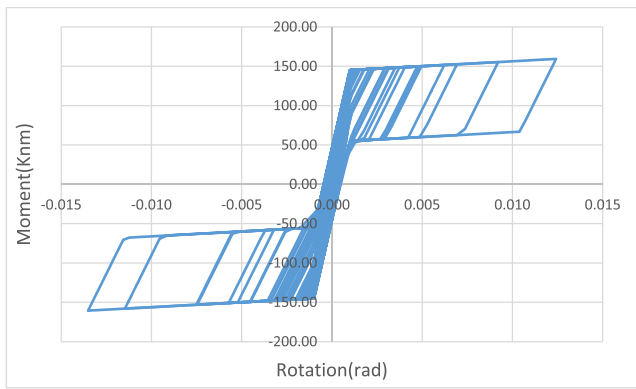


Fig. 23. Hysteresis curve of the combined effect of PC frame with friction dampers under Loma Prieta earthquake on the first floor of the 5-story building.

model structures is considered satisfactory when the mean response of the seven analysis results satisfies the given performance limit state. In this study, the limit state is determined such that the maximum inter-story drift is less than 2% of the story height, which is considered compatible with the LS limit state.

Fig. 22 shows the roof displacement time-histories of the 3, 5, and 8 story model structures for selected earthquakes. The figure shows that the retrofitted structures are experiencing less maximum roof displacements in general compared to the bare structures. The reduction reaches more than 50% in the case of the three-story building under the Chi-Chi earthquake. In addition, the residual drift has been reduced or eliminated in some cases as shown in Fig. 22(a). Fig. 23 shows the flag-shaped hysteretic behavior of the combined effect of self-centering and energy dissipation components of the PC frame on the first story of the 5-story building. This ensures the efficient self-centering and energy dissipation capabilities of the PC frame with the corner friction-damper retrofit technique.

Fig. 24 shows the maximum inter-story drift ratios (MIDR) of the

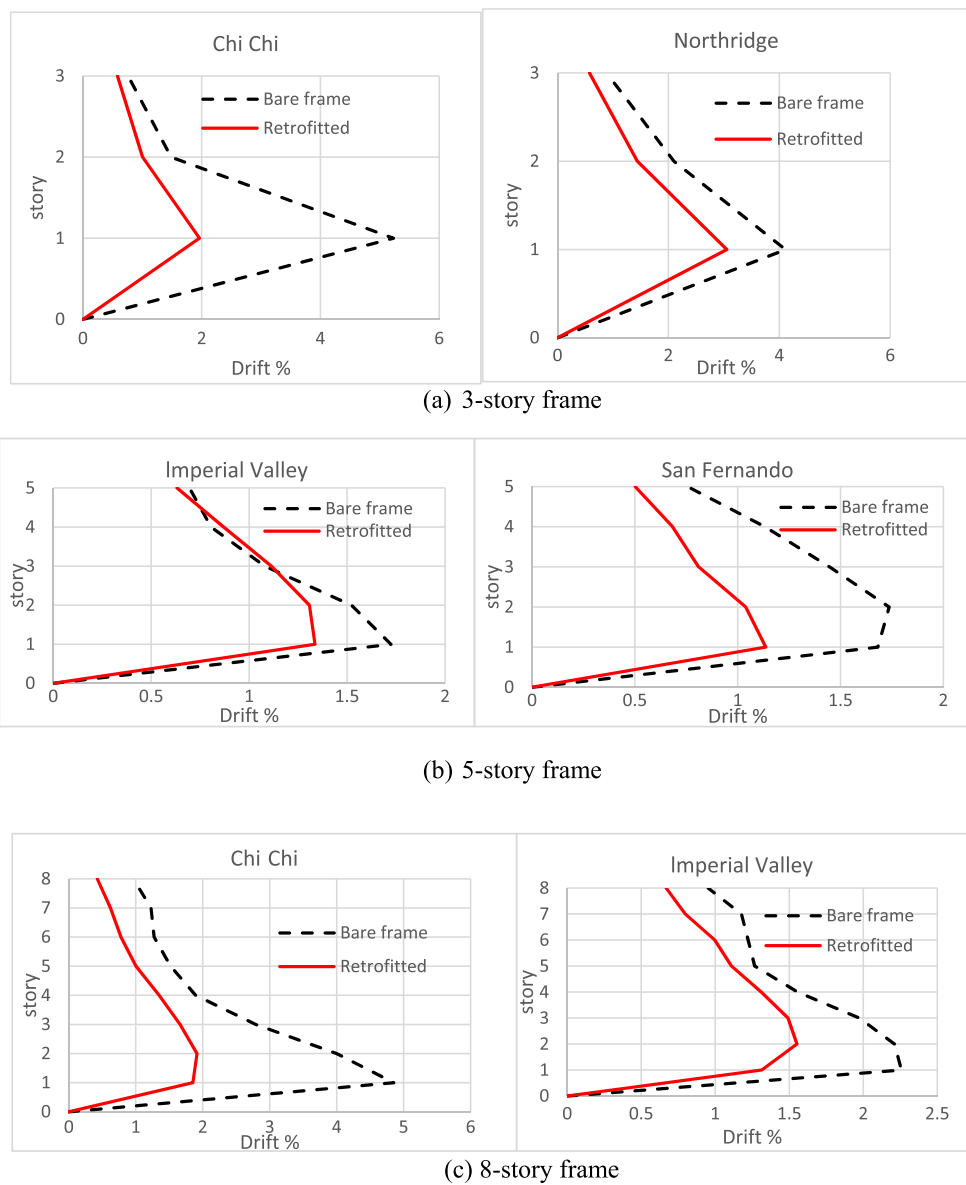


Fig. 24. Maximum inter-story drifts obtained from time history analyses.

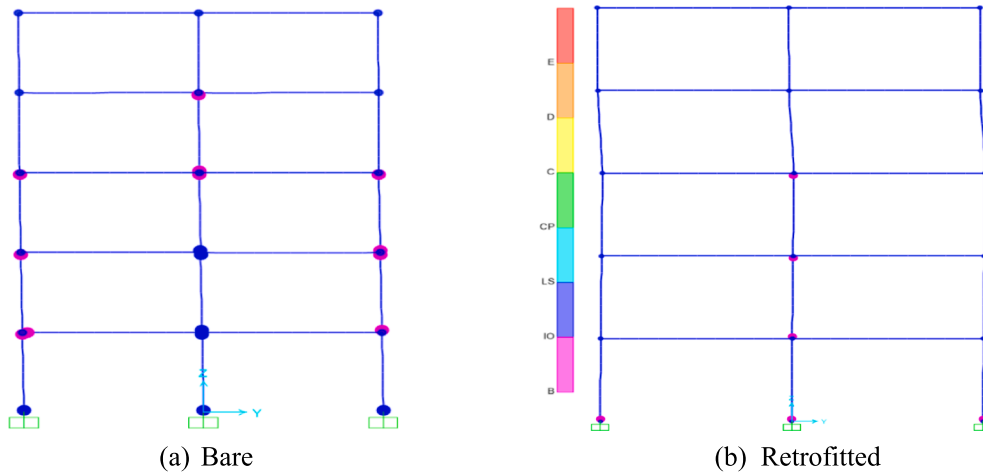


Fig. 25. Plastic hinge formation in the 5-story model structures before and after retrofit.

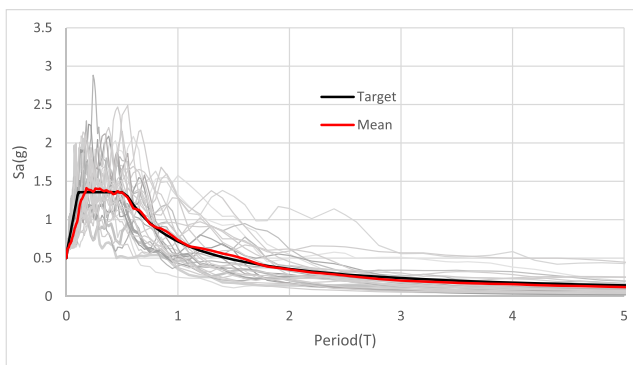


Fig. 26. Response spectra of the 30 ground motion records used for IDA.

model structures obtained from the nonlinear dynamic analyses. In the case of the 3-story building under the Chi-Chi earthquake, the MIDR is reduced from more than 5% to around 2%. In the case of the 5-story building under the San-Fernando earthquake, the reduction in MIDR was from 1.75% to 1.15%. In the case of the 8-story building under the Chi-Chi earthquake, the MIDR is reduced from 4.9% to 1.95%. This means that the PC frame with corner friction dampers as a seismic retrofit device is effective in decreasing the seismic response of framed structures below given limit states. Fig. 25 shows the plastic hinge distribution in the 5-story RC frame subjected to the San-Fernando earthquake before and after the seismic retrofit. It can be observed that both the number of plastic hinges and their rotations are significantly reduced after the seismic retrofit.

6.4. Evaluation of seismic fragility curves

In this section, 30 ground motion records obtained from the PEER NGA Database [26] are used to conduct incremental dynamic analyses (IDA) and to compute the probability of reaching given limit states of the analysis model structures. Fig. 26 shows the response spectra of the ground motions. IDA curves are constructed by conducting nonlinear

dynamic analysis using the set of ground motion scaled to specific intensity-measure in increasing order until reaching collapse or dynamic instability is encountered. Fig. 27 shows the IDA curves of the selected model structures before and after the retrofit. Each dot on the IDA curve represents the response of an earthquake scaled to the specific intensity level. It can be observed that the retrofitted structures show better performance compared to the un-retrofitted structures. The difference in the seismic performance can be highlighted in a better way through the seismic fragility curves. IDA curve is a first step to construct seismic fragility curves that provide a visual understanding of the probability of a structure to reach a given damage state. The probability of the structural capacity being less than the seismic demand for a specific limit state is related to the seismic measure intensity through a conditional probability lognormal cumulative distribution function [27]:

$$P[C < D@SI = x] = 1 - \Phi\left[\frac{\ln(\hat{C}/\hat{D})}{\beta_{TOT}}\right]$$

12

where C is the structural capacity; D is the structural demand; SI is the seismic intensity hazard; $\Phi[.]$ is the standard normal probability integral; \hat{C} is the median structural capacity for a specific limit state; \hat{D} is the median structural demand; β_{TOT} is the total system collapse uncertainty, which is taken to be 0.6 based on the FEMA P695 [28] recommendation. The fragility curves are constructed based on the IDA curves and the above equation. At every spectral acceleration on the vertical axis of the IDA curve, the median of the structural demand of all earthquakes is calculated. After that, this value is used in the above equation to obtain the probability of reaching or exceeding a specific limit state that corresponds to each spectral acceleration.

Fig. 28 shows the fragility curves of the bare and retrofitted frames at three damage states: (a) IO, (b) LS, and (c) CP, which corresponds to MIDR of 1%, 2%, and 3%, respectively. As can be observed from the figure, the retrofitted buildings show smaller seismic fragility than the un-retrofitted ones. For example, for the 3-story building, the improvement is manifested for the three limit states. In addition, the improvement in the fragility for the LS and CP limit states is higher than that of the IO limit state at the 50% probability of exceedance. This indicates that for low-rise structures similar to the buildings selected in the current study, the retrofit technique is more effective for higher

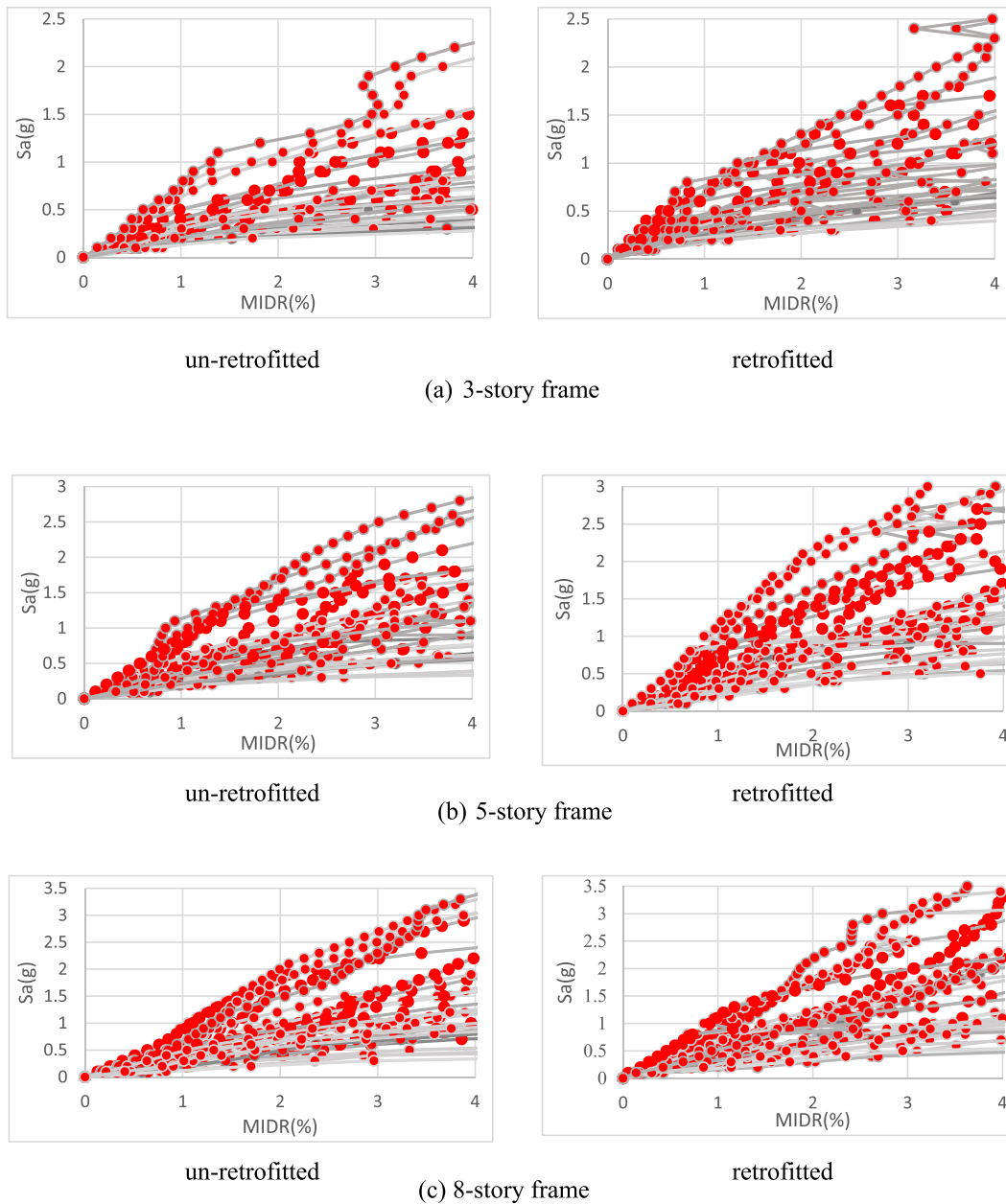


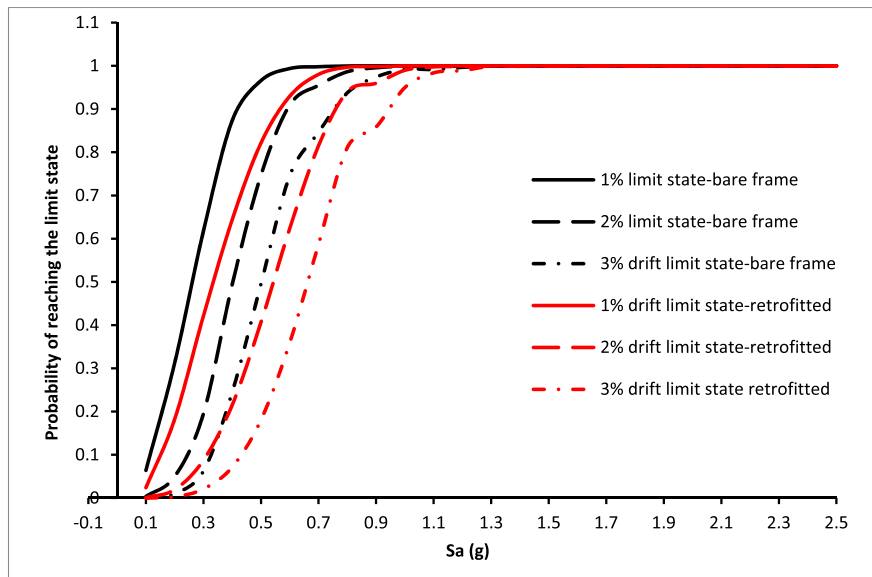
Fig. 27. IDA curves of the analysis model structures.

limit states, such as LS and CP in comparison with lower-level limit states, such as IO. For the 5-story building, the fragilities of the retrofitted buildings are lower, in general, than those of the un-retrofitted ones. However, the improvement is more pronounced for the LS and CP limit states in comparison with the IO limit state. The increase in the spectral acceleration at the 50% probability of exceedance is found to be 0.07 g, 0.15 g, and 0.16 g, respectively, for the IO, LS, and CP limit states. In the 8-story structure, the fragilities follow the same pattern observed in the 5-story structure. The increase in the spectral acceleration at the 50% probability of exceedance is 0.06 g, 0.16 g, and 0.22 g, respectively, for the IO, LS, and CP limit states. This means that

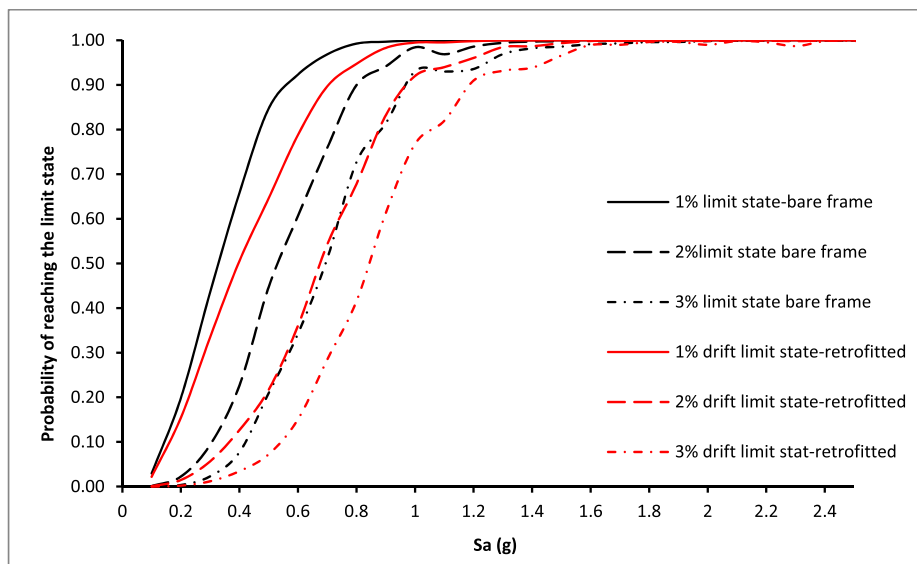
the largest increase is found in the CP limit state.

7. Conclusion

In this study, a seismic retrofit scheme was proposed using a pre-loaded PC frames with corner friction dampers attached externally to existing RC structures. Cyclic loading tests were conducted on RC frame specimens to validate the effectiveness of the retrofit scheme, and the experimental results are used to validate the numerical modeling of the test specimens. A design procedure was proposed based on a genetic algorithm (GA) to obtain the optimum design parameters of the PC



(a) 3-story frame



(b) 5-story frame

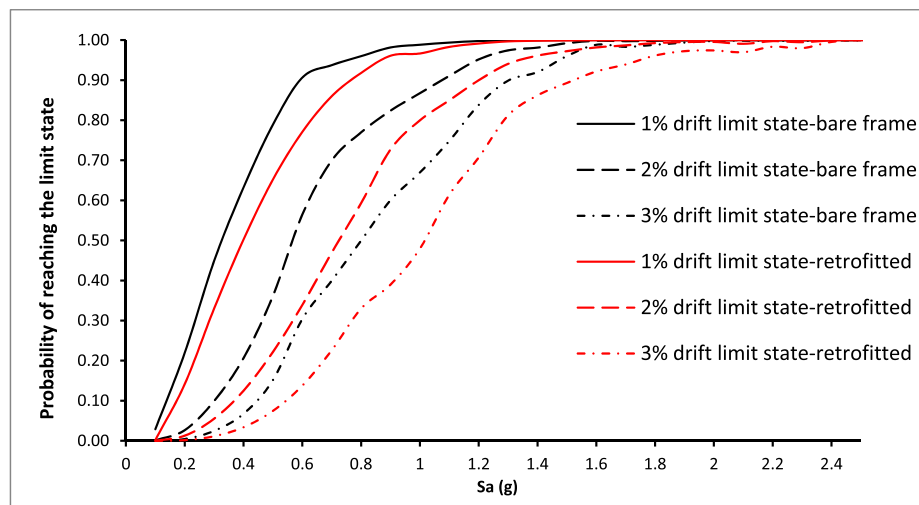
Fig. 28. Fragility curves before and after retrofit at three damage states (IO = 1.0%, LS = 2.0%, and CP = 3.0%).

frame and the optimum yield force of the friction dampers. Three framed structures were simulated numerically to investigate the effectiveness of the proposed retrofit in terms of inter-story drift and seismic fragility.

According to the dynamic analysis using seven different earthquakes, after the seismic retrofit using the proposed system the maximum roof displacements were reduced as much as approximately 60% in the case of 3- and 8-story model structures and 34% in the 5-story structure. The incremental dynamic analyses using thirty different earthquakes showed that the retrofit scheme was effective in increasing the collapse capacities of the model structures, and the seismic fragility

analyses showed that the proposed retrofit technique was more effective in decreasing failure probability especially for the higher limit states such as LS and CP.

Finally, it needs to be pointed out that the proposed retrofit system is intended to enhance the seismic fragility and collapse capacity of the superstructure; however, the retrofit may increase the demands for base shear and the reaction force on the foundation system. Therefore after the seismic retrofit of the super structure, the safety of the foundation needs to be checked and proper reinforcement should be provided if necessary.



(c) 8-story frame

Fig. 28. (continued)

Declaration of Competing Interest

The authors confirm that there is no conflict of interest in the paper submitted.

Acknowledgment

This research was carried out by research funding (task number 19CTAP-C153076-01) of the Ministry of Land, Infrastructure and Transport, Land Transport Technology Promotion Research Project.

References

- [1] Christopoulos C, Filiatrault A, Uang CM, Folz B. Post-tensioned energy dissipating connections for moment-resisting steel frames. *J Struct Eng* 2002;1111–20. [https://doi.org/10.1061/\(ASCE\)0733-9445\(2002\)128:9\(1111\)](https://doi.org/10.1061/(ASCE)0733-9445(2002)128:9(1111)).
- [2] Morgen B, Kurama YC. A friction damper for posttensioned precast concrete moment frames. *PCI J* 2004;49(4):112–33.
- [3] Naeem A, Eldin MN, Kim J, Kim J. Seismic performance evaluation of a structure retrofitted using steel slit dampers with shape memory alloy bars. *Int J Steel Struct* 2017;17(4):1627–38.
- [4] Roke D, Sause R, Ricles JM, Chancellor B. (2013), Damage-Free Seismic-Resistant Self-Centering Concentrically-Braced Frames, <https://nees.org/resources/6727>.
- [5] Eatherton M, Ma X, Krawinkler H, Deierlein GG, Hajjar JF. Quasi-static cyclic behavior of controlled rocking steel frames. *J Struct Eng* 2014;140(11).
- [6] Cui Y, Lu X, Jiang C. Experimental investigation of tri-axial self-centering reinforced concrete frame structures through shaking table tests. *Eng Struct* 2017;132:684–94.
- [7] Akbas T, Sause R, Ricles JM, Ganey R, Berman J, Loftus S, et al. Analytical and experimental lateral-load response of self-centering post-tensioned CLT walls. *J Struct Eng* 2017;143(6):04017019.
- [8] Shu Z, Li Z, He M, Zheng X, Wu T. Seismic design and performance evaluation of self-centering timber moment resisting frames. *Soil Dyn Earthquake Eng* 2019;119:346–57.
- [9] Song LL, Guo T, Chen C. Experimental and numerical study of a self-centering prestressed concrete moment resisting frame connection with bolted web friction devices. *Earthquake Eng Struct Dyn* 2013;43(4).
- [10] Cao Z, Guo T, Xu Z, Lu S. Theoretical analysis of self-centering concrete piers with external dissipators. *Earthquakes Structures Int J* 2015;9(6).
- [11] Guo T, Xu Zhenkuan, Song Lianglong, Wang Lei. Seismic resilience upgrade of RC frame building using self-centering concrete walls with distributed friction devices. *J Struct Eng* 2017.
- [12] Dezfuli MA, Dolatshahi KM, Mofid M, Eshkevari SS. Coreless self-centering braces as retrofit devices in steel structures. *J Constr Steel Res* 2017;133:485–98.
- [13] NourEldin M, Naeem Asad, Kim Jinkoo. Seismic retrofit of a structure using self-centering precast concrete frames with enlarged beam ends. *Mag Concr Res* 2019. <https://doi.org/10.1680/jmacr.19.00012>.
- [14] Morelli F, Piscini A, Salvatore W. Seismic behavior of an industrial steel structure retrofitted with self-centering hysteretic dampers. *J Constr Steel Res* 2017;139:157–75. <https://doi.org/10.1016/j.jcsr.2017.09.025>.
- [15] Morelli F, Piscini A, Salvatore W. Development of an asymmetric re-centering dissipative device. *J Constr Steel Res* 2019;161:227–43. <https://doi.org/10.1016/j.jcsr.2019.07.004>.
- [16] Mattock AH. Flexural strength of prestressed concrete sections by programmable calculator. *PCI J* 1979;24(1):26–37.
- [17] ACI 374.2r-13. Guide for testing reinforced concrete structural elements under slowly applied simulated seismic loads, USA; 2013.
- [18] Celik O, Sritharan S. An evaluation of seismic design guidelines proposed for precast concrete hybrid frame systems. ISU-ERI-Ames Report ERI-04425, Submitted to the Precast/Prestressed Concrete Manufacturers Association of California, Final report. Iowa State University of Science and Technology.
- [19] McKenna F, Fenves GL, Scott MH. Open system for earthquake engineering simulation. Berkeley, CA: Univ. of California; 2000.
- [20] SAP2000, ver. 18. Analysis Reference Manual. Computer and Structures, Berkeley, USA; 2015.
- [21] American Concrete Institute (ACI). Building Code Requirements for Structural Concrete (ACI 318-14) and Commentary (ACI 318R-14), Michigan, USA; 2014.
- [22] ASCE. Seismic evaluation and retrofit of existing buildings. ASCE41-13; 2013.
- [23] Rahman MA, Sritharan S. Performance-based seismic evaluation of two five-story precast concrete hybrid frame buildings. *J Struct Eng* 2007;133:11.
- [24] Chao SH, Goel SC, Lee SS. A seismic design lateral force distribution based on inelastic state of structures. *Earthquake Spectra* 2007;23(3):547–69.
- [25] ASCE/SEI 7, 2016. Minimum design loads for buildings and other structures. USA: American Society of Civil Engineers.
- [26] PEER. Pacific Earthquake Engineering Research (PEER) Center: NGA Database. Retrieved April 8, 2019, from <http://peer.berkeley.edu/nga/>.
- [27] Celik OC, Ellingwood BR. Seismic risk assessment of gravity load designed reinforced concrete frames subjected to Mid-America ground motions. *J Struct Eng* 2009;135(4):414–24. [https://doi.org/10.1061/\(ASCE\)0733-9445\(2009\)135:4\(414\)](https://doi.org/10.1061/(ASCE)0733-9445(2009)135:4(414)).
- [28] FEMA P695. Quantification of building seismic performance factors. Washington (DC, USA): Federal Emergency Management Agency; 2009.